Near-barrier fusion of $^{36}S+^{90,96}Zr$: The effect of the strong octupole vibration of ^{96}Zr

A. M. Stefanini, L. Corradi, A. M. Vinodkumar, and Yang Feng*
Istituto Nazionale di Fisica Nucleare, Laboratori Nazionali di Legnaro, I-35020 Legnaro, Padova, Italy

F. Scarlassara, G. Montagnoli, S. Beghini, and M. Bisogno
Dipartimento di Fisica, Universitá di Padova and Istituto Nazionale di Fisica Nucleare, Sezione di Padova, I-35131, Padova, Italy

(Received 30 November 1999; published 26 May 2000)

Fusion-evaporation cross sections have been measured for $^{36}S+^{90,96}Zr$ to high accuracy near the Coulomb barrier. The sub-barrier cross sections for $^{36}S+^{96}Zr$ are much larger compared to $^{36}S+^{90}Zr$. The extracted fusion barrier distributions have different shapes, with essentially one peak for $^{36}S+^{90}Zr$, and a wider and more complex structure for $^{36}S+^{96}Zr$. Coupled-channels calculations explain the larger sub-barrier enhancement for $^{36}S+^{96}Zr$ as due mainly to the strong octupole vibration in ^{96}Zr. However, the calculations do not reproduce well the barrier distribution for this system. The comparison with $^{40}Ca+^{90,96}Zr$ suggests that couplings to nucleon transfer channels may play a role in the large enhancement of sub-barrier fusion for $^{40}Ca+^{96}Zr$.

PACS number(s): 25.70.Jj, 24.10.Eq, 27.60.+j

I. INTRODUCTION

The dynamics of heavy-ion fusion in the energy range near and below the Coulomb barrier has been the object of considerable interest and of many experimental and theoretical studies in recent years. Following the early suggestion of Rowley *et al.* [1], a representation of the fusion barrier distribution arising from couplings to reaction channels, may be obtained, within some approximations, from the second derivative of the excitation function with respect to the energy. That procedure has indeed allowed a deep insight on the fusion dynamics for several heavy-ion systems, which would not have been possible from the simple analysis of excitation functions and from their comparison with theoretical models (recent reviews in this field can be found in Refs. [2,3]).

A detailed study of the two systems $^{40}Ca+^{90,96}Zr$ was performed recently [4]. Since the projectile ^{40}Ca is a magic nucleus, its influence on fusion was expected to be easily calculated; moreover, both targets $^{90,96}Zr$ have a $Z=40$ subshell closure. But a main difference between those two reactions is in the neutron transfer Q values which are very positive, in the case of ^{96}Zr only, up to the pickup of eight neutrons. Furthermore, the low-lying quadrupole vibrations of ^{90}Zr and ^{96}Zr are found at similar excitation energies and are only moderately collective, but ^{96}Zr has a strong octupole vibration, much stronger and lower in energy than the corresponding one in ^{90}Zr.

A very large relative enhancement was observed for $^{40}Ca+^{96}Zr$ low-energy fusion compared to $^{40}Ca+^{90}Zr$; in addition, the barrier distribution for ^{96}Zr is flat and almost structureless, and extends to very low energies. It is qualitatively different from the distribution for ^{90}Zr which shows well-defined peaks. The barrier distribution and fusion excitation function of $^{40}Ca+^{90}Zr$ could be explained in terms of couplings to the low-lying inelastic excitations of ^{90}Zr, but the analogous calculations for $^{40}Ca+^{96}Zr$ failed completely. This was interpreted as an indication that neutron transfer may be important to enhance sub-barrier fusion in $^{40}Ca+^{96}Zr$.

Therefore, it is important to assess experimentally the effect of the strong octupole vibration of ^{96}Zr on fusion. That is surely a concurring reason for the relative enhancement of $^{40}Ca+^{96}Zr$ compared to $^{40}Ca+^{90}Zr$, since, qualitatively, one expects that the octupole shape strongly favors sub-barrier fusion. The case of $^{36}S+^{96}Zr$ appears to be interesting, since the 3^- state is relatively low and very strong, and, on the other hand, all neutron transfer Q values are large and negative. Hence, if those transfer channels are important in $^{40}Ca+^{96}Zr$, we expect for $^{36}S+^{96}Zr$ less sub-barrier fusion, and a different barrier distribution with, possibly, separated peaks; the effect of octupole coupling may be unambiguously identified.

We report here about the measurement of near- and sub-barrier fusion of $^{36}S+^{90}Zr$ and $^{36}S+^{96}Zr$, done with small energy steps and good statistical accuracy, so as to extract the barrier distribution from the second derivative of the excitation functions. The fusion cross sections of $^{36}S+^{90}Zr$ were measured as well; this system has very similar characteristics to $^{40}Ca+^{90}Zr$, hence one expects a similar behavior in the sub-barrier fusion. These two systems should constitute a common basis ''on top of which'' the enhancements and particular effects due to neutron transfer and/or to octupole vibrations are built up.

This paper is organized as follows: Sec. II presents the setup and the measurements, together with the experimental data; Sec. III reports about the analysis of the data within the coupled-channel model; in Sec. IV a full comparison is done with the previous data for $^{40}Ca+^{90,96}Zr$, and conclusions will be drawn in Sec. V.

II. EXPERIMENTAL

The experiments have been performed at the XTU Tandem accelerator of the Laboratori Nazionali di Legnaro of

*On leave from the China Institute of Atomic Energy, 102413 Beijing, China.

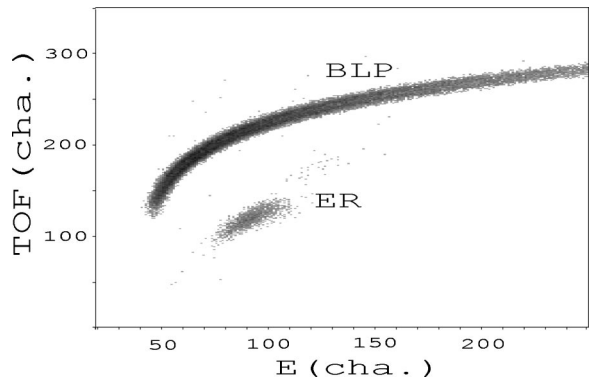

FIG. 1. Two-dimensional plot *E*-TOF of the events, following beam separation, taken at $E_{lab}=111.1$ MeV and at 0°, for the $^{36}S+^{96}Zr$ reaction. Two groups of ions [beam-like particles (BLP) and evaporation residues (ER)] are indicated. A few events are also seen between the two main groups, which come from a slight contamination of the ^{96}Zr target.

INFN. The ^{36}S beam was produced by a sputter ion source where a AgS sample was introduced, with Sulphur enriched to around 50% in mass 36. The accelerated beams of ^{36}S had energies in the range 99.2–123.0 MeV, and the targets were evaporations of $^{90}ZrO_2$ (60 $\mu g/cm^2$) and $^{96}Zr_2O_3$ (90 $\mu g/cm^2$) on carbon layers 20 $\mu g/cm^2$ and 15 $\mu g/cm^2$ thick, respectively; the carbon backings faced the beam. Typical beam intensities ranged between 10 and 20 pnA. The target isotopic enrichments were 99.36% and 95.63% for ^{90}Zr and ^{96}Zr, respectively; these values were used, together with the target compositions, to introduce small corrections to the measured cross sections.

An electrostatic deflector [5] separated the forward recoiling evaporation residues (ER) from the transmitted beam and beamlike particles. A beam rejection factor at 0° routinely around 10^8 was achieved. The ER were then identified by a time-of-flight (TOF)-energy (*E*) telescope consisting of a microchannel plate detector and (40 cm downstream) of a 300 mm^2 silicon surface-barrier detector; the geometrical solid angle of the telescope was $\simeq 0.025$ msr. Figure 1 is an *E*-TOF two-dimensional spectrum where the ER events and the beamlike particles (BLP) are clearly separated.

Four monitor detectors were placed at $\theta \simeq 17°$, symmetrically around the beam direction; this allowed us to establish, for each run, the beam direction very accurately (to within 0.1°) and small deviations from the nominal 0° were taken into account in the data reduction. The position of the beam spot ($\phi \simeq 1.5$ mm) on the target affects as well the relative counts of the monitors and the corresponding correction is possible; a quartz viewer, allowing one to appreciate beam shifts as small as 0.3 mm, was used at the beginning and at the end of each run to check that position (normally very stable).

Special care was devoted to the beam quality (see [6] for a more complete discussion about this point). In order to minimize hysteresis effects in the energy-defining magnet, both 0° excitation functions were measured in a single sequence of runs with energy steps $\Delta E_{lab}=700$ keV, starting from the highest energy 123 MeV. Apart from the carbon backings, the beam energy losses in the whole thickness of the $^{90,96}Zr$ targets were $\simeq 600-900$ keV, depending on the energy and on the isotope. Therefore, the measured cross sections are averaged over that energy range which is substantially larger, anyway, than the maximum uncertainty in the absolute beam energy ($\simeq 130$ keV at 100 MeV) [7].

ER angular distributions were measured for both targets at $E_{lab}=107.6$ and 118.1 MeV in the range $-6°$ to $+4°$ in steps of 1°. As in previous experiments on near-barrier fusion (see [4] and references therein), no significant energy dependence of the width and shape of the angular distributions has been observed. The angular distributions are nicely symmetrical around the nominal 0° and drop by a factor ≈ 100 at 6°. The total fusion-evaporation cross sections (fusion-fission is negligible) have been derived by integrating those distributions and by a simple inter(extra)polation procedure for all other energies. Overall, the absolute cross section scale is accurate within $\pm 15\%$; contributions to the systematic errors come from the geometrical solid angle uncertainties, from the angular distribution integrations and, mainly, from the transmission of the electrostatic deflector, which was determined to be 0.56 ± 0.06 for both systems $^{36}S+^{96,90}Zr$ by Montecarlo simulations (see [8] for more details). The cross sections measured in this work are listed in Table I and Fig. 2 shows both experimental excitation functions in a modified energy scale (see caption). $^{36}S+^{96}Zr$ has sub-barrier cross sections larger by at least one order of magnitude with respect to $^{36}S+^{90}Zr$.

III. DATA ANALYSIS

A first step in the data analysis has been the extraction of the fusion barrier distributions as the second energy derivatives of the excitation functions. The usual three-point difference formula has been applied [4], and the best compromise between accuracy and sensitivity was found with an energy step $\Delta E=1.5$ MeV. The corresponding distributions are shown in the lower panels of Figs. 3 and 4; the plotted quantities D_{fus} are the second energy derivatives of the excitation functions, divided by πR_b^2, where R_b is the barrier radius obtained from the standard Akyüz-Winther potential [9]. A complex broad structure is seen for $^{36}S+^{96}Zr$ extending in the range $\simeq 72-79$ MeV. One single peak is observed for $^{36}S+^{90}Zr$ at $E_{c.m.} \simeq 77$ MeV, with, possibly, a second structure at ≈ 80 MeV.

Table II contains the relevant information on the low-lying states of ^{36}S, ^{90}Zr, and ^{96}Zr included in the coupled-channels calculations described below. The ^{36}S inelastic excitations lie at rather high excitation energies; the 2^+ state is at 3.291 MeV, and the lowest 3^- state is at 4.192 MeV. The quadrupole vibration is relatively weak ($\beta=0.16$), whereas the octupole strength is not known experimentally [10]. As far as the two isotopes $^{90,96}Zr$ are concerned [11–13], the quadrupole vibrations are weak and do not differ much in the two Zr isotopes, but we notice in particular the strong octupole vibration of ^{96}Zr, where a deformation parameter even larger ($\beta_3=0.295$) has been recently reported [14]. In this

TABLE I. Fusion cross sections for $^{36}S+^{90,96}Zr$ measured in this work. The energies E are in the center-of-mass system; quoted errors are pure statistical uncertainties.

$^{36}S+^{90}Zr$				$^{36}S+^{96}Zr$			
E (MeV)	σ_{ER} (mb)	E (MeV)	σ_{ER} (mb)	E (MeV)	σ_{ER} (mb)	E (MeV)	σ_{ER} (mb)
73.7	0.090±0.021	81.2	176.5±3.4	71.1	0.067±0.011	79.7	220.9±3.8
74.2	0.18±0.05	81.7	207.5±4.1	71.6	0.22±0.05	80.2	249.0±4.3
74.7	0.88±0.07	82.2	223.1±4.2	72.1	0.27±0.05	80.8	273.7±4.8
75.2	2.28±0.16	82.7	251.5±4.8	72.6	1.45±0.10	81.3	300.4±4.9
75.7	4.85±0.27	83.2	273.4±5.3	73.1	3.88±0.16	81.8	326.2±5.6
76.2	9.12±0.30	83.7	299.6±5.5	73.6	9.65±0.31	82.3	344.7±6.1
76.7	17.4±0.77	84.2	317.6±4.8	74.2	16.6±0.44	82.8	368.7±6.2
77.2	27.3±0.70	84.7	357.4±5.4	74.7	26.4±0.65	83.3	387.1±7.1
77.7	42.5±1.0	85.1	367.6±4.7	75.2	35.3±0.80	83.8	400.6±6.5
78.2	61.9±1.2	85.7	392.2±5.2	75.7	47.4±1.0	84.3	434.0±7.3
78.7	80.8±1.6	86.2	411.5±5.8	76.2	67.4±1.4	84.8	453.5±6.6
79.2	97.5±1.9	86.7	425.1±6.4	76.7	82.8±1.8	85.4	482.4±6.2
79.7	117.0±2.2	87.2	469.7±5.0	77.2	95.9±1.7	85.9	504.4±6.8
80.2	140.2±3.8			77.7	122.0±2.4	86.4	543.4±7.5
80.7	161.5±3.0			78.2	147.5±2.1	86.7	545.8±5.7
				78.7	176.0±3.1	87.4	586.2±6.6
				79.2	200.3±2.5		

paper we use the original parameter $\beta_3=0.27$, since it gives a better fit to the data.

It is expected that nucleon transfer channels do not play any important role for the dynamics of sub-barrier fusion, since, for both $^{36}S+^{90}Zr$ and $^{36}S+^{96}Zr$, all ground-state Q values are large and negative, in a close analogy to the case of $^{40}Ca+^{90}Zr$. For $^{36}S+^{90}Zr$ only, positive Q values are found for proton pickup channels. The larger sub-barrier fusion cross sections measured for $^{36}S+^{96}Zr$ (Fig. 2) are probably due to the strong 3^- state of ^{96}Zr.

The theoretical analysis has been performed within the coupled-channels (CC) approach, using the code CCFULL [15]. This program employs the isocentrifugal approximation in order to reduce the number of coupled-channels equations,

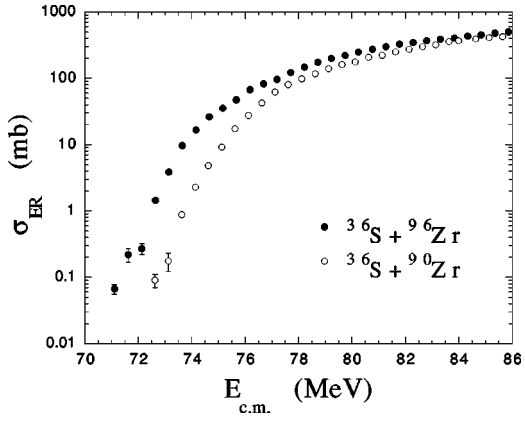

FIG. 2. The excitation functions measured in this work; the data for $^{36}S+^{90}Zr$ has been shifted to lower energies by 1.1 MeV, to take approximate account of the difference in the nominal Coulomb barrier with respect to $^{36}S+^{96}Zr$. The error bars are statistical uncertainties only.

and it uses the incoming-wave boundary condition inside the barrier. It takes account of the finite excitation energies of the coupled modes and it includes the effects of inelastic nonlinear couplings to all orders. It is actually known [16–18] that linear couplings and the adiabatic approximation are inadequate to the description of heavy-ion sub-barrier fusion, in particular for heavy systems. Vibrational couplings, like the case of the heavy-ion systems studied in the present work, are treated by CCFULL in the harmonic-oscillator limit.

The Akyüz-Winther (bare) potential parameters are reported in Table III, together with those of the modified ion-ion potential that we have used for the CC calculations. As far as the diffuseness is concerned, the value $a=0.9$ fm has been used like in other cases studied recently [4,19]; it seems actually a systematic trend that large values of the diffusivity are needed to fit the high-energy part of the fusion excitation functions, and this fact is still awaiting a full explanation.

The following observations are also important in this context: the peak in the barrier distribution for $^{36}S+^{90}Zr$ is rather sharp, with a full width at half maximum $\simeq 2.4$ MeV; this means, taking into account the smoothing introduced by the finite-difference formula, that the curvature of the barrier should be $\hbar\omega\approx 3.35$ MeV. This is smaller than what is obtained by the standard Akyüz-Winther potential ($\hbar\omega\simeq 3.70$ MeV), thus indicating that a diffuseness larger than $a=0.67$ fm should be used. The rather steep slopes of the excitation functions at very low energies also point in this direction.

The potential well has been chosen to be deep ($V_0=200$ MeV) in order to avoid oscillations in the trasmission coefficients of high partial waves, especially at energies above the Coulomb barrier. Accordingly, the radius parameter r_0 has been reduced, so as to reproduce the high-energy part of the excitation functions. We have used $r_0=1.01$ (0.99) fm

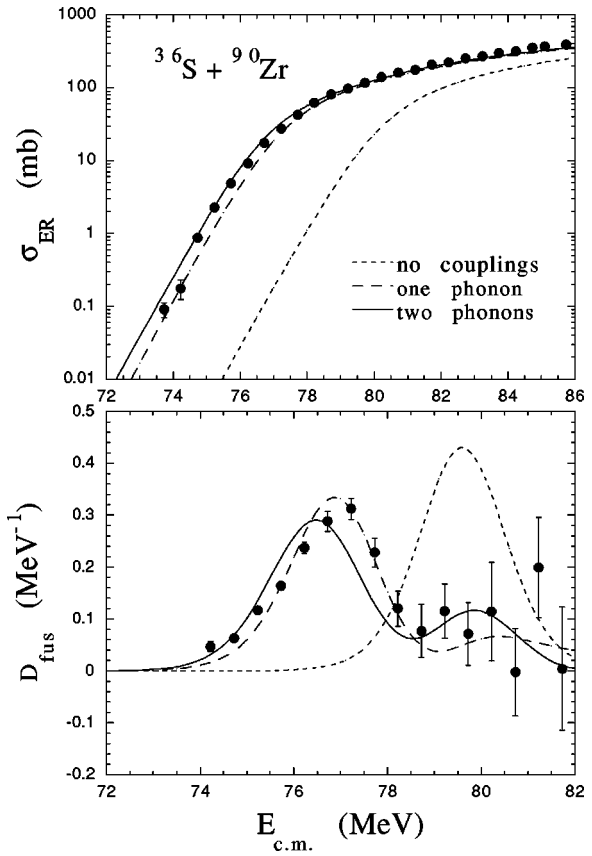

FIG. 3. Excitation function (upper panel) and barrier distribution (lower panel) for $^{36}S+^{90}Zr$, in comparison with coupled-channels calculations performed with the code CCFULL [15]; see text for details. The reported errors derive from statistical uncertainties only. The energy scale is expanded in the lower panel.

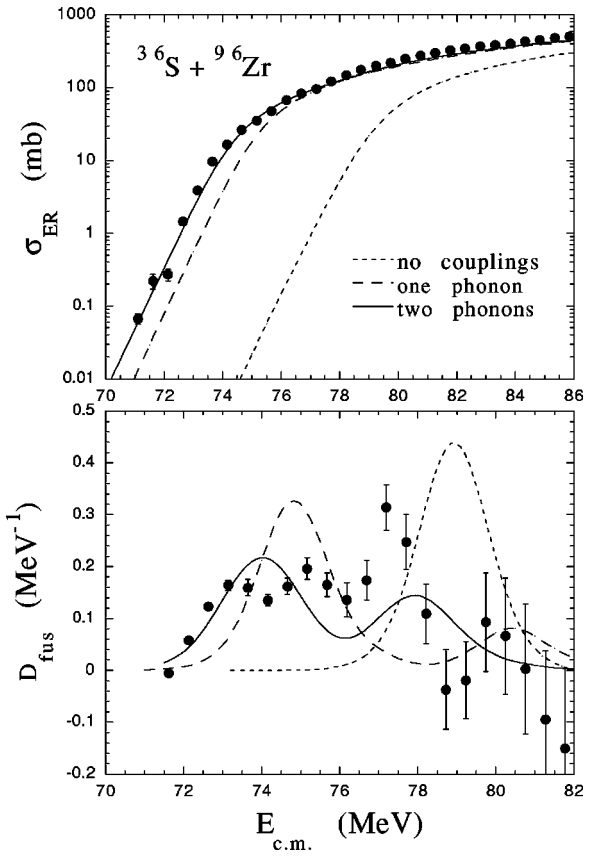

FIG. 4. Excitation function and barrier distribution for $^{36}S+^{96}Zr$, in comparison with coupled-channels calculations performed with the code CCFULL; see text for details. The reported errors derive from statistical uncertainties only. The energy scale is expanded in the lower panel.

for $^{36}S+^{96(90)}Zr$: the difference between the two systems has no particular meaning, since it may easily be due to the uncertainty in our absolute cross section scales (see preceding section).

We point out that the lowest 3^- state of ^{36}S has an excitation energy (4.192 MeV) substantially higher than $\hbar\omega$; hence its effect on the dynamics is a simple renormalization of the bare potential, leaving untouched the structure of the barrier distribution, by an amount which is unknown *a priori*, since the coupling strength of that level to the ground state is not known. Also in view of this, we preferred not to use the Akyüz-Winther potential for the CC calculations, but the modified one described above, which already includes the effect of the 3^- state of ^{36}S.

The fusion barriers produced by the Akyüz-Winther potential are shown in the lower panel of Table III, as are the corresponding values from the potential used for the CC calculations.

The results of the CCFULL calculations for $^{36}S+^{90}Zr$ are shown in Fig. 3; the no-coupling limit, calculated with the Akyüz-Winther potential, is shown as well. The coupled modes are the 2^+ state of ^{36}S, and the 2^+ and 3^- states of ^{90}Zr, with the deformation parameters listed above. The relatively strong 5^- state of ^{90}Zr at 2.319 MeV was included (as in Ref. [4]) by adding in quadrature its strength to that of the quadrupole vibration. The dashed lines show what one obtains by considering one-phonon vibrations only, for each of these modes, and by including the $2^+\otimes 3^-$ excitation of the target nucleus as well (CCFULL also takes account automatically of the mutual target-projectile excitations); the solid lines are the results of the further calculation where, in addition, the octupole double phonon $(3^-)^2$ state of ^{90}Zr was included, together with its combined excitation with the quadrupole vibrations. The effects of two-phonon quadrupole couplings have been checked to be very small.

Both lines give a reasonably good account of the experi-

TABLE II. Excitation energies E_x, spin and parities λ^π, and deformation parameters β_λ of the states included in the coupled-channels calculations (see text).

Nucleus	E_x(MeV)	λ^π	β_λ
^{36}S	3.291	2^+	0.16
	4.192	3^-	
^{90}Zr	2.186	2^+	0.09
	2.748	3^-	0.22
	(2.319	5^-	0.12)
^{96}Zr	1.751	2^+	0.08
	1.897	3^-	0.27

TABLE III. The upper panels show, for the two studied systems, the parameters of the Akyüz-Winther potential and of the modified potential used for the CC calculations (see text). In the lower panels the resulting fusion barriers (height, radius, and curvature) are reported.

Potential	$^{36}S+^{90}Zr$			$^{36}S+^{96}Zr$		
	V_o (MeV)	r_o (fm)	a (fm)	V_o (MeV)	r_o (fm)	a (fm)
Akyüz-Winther	69.76	1.177	0.668	69.74	1.177	0.670
CC-potential	200.0	0.99	0.90	200.0	1.01	0.90
	V_b (MeV)	r_b (fm)	$\hbar\omega$ (MeV)	V_b (MeV)	r_b (fm)	$\hbar\omega$ (MeV)
Akyüz-Winther	79.8	10.76	3.72	78.9	10.90	3.65
CC-potential	79.0	10.64	3.32	77.2	10.92	3.22

mental results; the comparison with the data does not help in deciding whether the second octupole phonon is really necessary, since this brings a better agreement of the calculations with the sub-barrier cross sections, but it worsens the fit of the barrier distribution to some extent.

The situation is different for ^{96}Zr, as shown in Fig. 4; the dotted, dashed and solid lines show the CCFULL calculations with no couplings, one- and two-phonon couplings, respectively, as described above for ^{90}Zr. Here again, the only two-phonon excitation with a significant effect on both cross sections and barrier distribution is the $(3^-)^2$ state of ^{96}Zr, and in this case it is essential for a good fit of the excitation function; this is due to the lower excitation energy and to the larger strength of the octupole vibration in ^{96}Zr, whose effect is clearly identified.

Nevertheless, the calculations give only a marginal fit of the barrier distribution shape; reproducing the low-energy part with the correct intensity compared to the main ''structure'' at $E \simeq 77.5$ MeV, would require coupling to positive Q-value transfer channels with significant strength, which are not available, and/or to a quadrupole vibration in ^{96}Zr with $\beta_2 \approx 0.3$, much stronger than the adopted value [14] for the lowest 2^+ state. The solid line in Fig. 4 (two-phonon calculation) reproduces correctly the overall width of the barrier distribution, but only qualitatively its shape. The one-phonon calculation does a worse job, anyway. No other inelastic excitations with significant strength are known in ^{96}Zr, hence the disagreement is at present unexplained. We have tried, also, to vary the potential parameters (diffuseness and radius, essentially), but no significant improvement of the barrier distribution fit has been found, while the good fit of the excitation function is rapidly destroyed, as expected, when the variations produce a different average fusion barrier.

One might argue that the disagreement for ^{96}Zr is due to the approximations of the CC code, i.e., the isocentrifugal approximation and the treatment of the inelastic excitations as pure harmonic oscillations. Actually, Hagino *et al.* [21] have recently shown that anharmonicities, like those existing in most vibrational nuclei, cause non-negligible effects in the calculated cross sections and barrier distributions. In that paper, a significant analysis of the data for $^{16}O+^{148}Sm$ [19] is done, by discussing the anharmonic properties of the quadrupole and octupole vibrations of ^{148}Sm.

The present situation for $^{36}S+^{96}Zr$ appears to be similar to what has been found recently for $^{16}O+^{208}Pb$ [22] where a full coupled-channels analysis of improved fusion data could not give any satisfactory and simultaneous description of the low-energy cross sections and of the barrier distribution shape.

As a summary of this section, we notice that the coupled-channels model gives a good account of the experimental data for $^{36}S+^{90}Zr$; the same theory fits well the excitation function of $^{36}S+^{96}Zr$, and here the role of the one- and two-phonon octupole vibration is dominant. However, the fusion barrier distribution of $^{36}S+^{96}Zr$ is only approximately reproduced by the same calculations, and this point needs further consideration.

IV. COMPARING WITH $^{40}Ca+^{90,96}Zr$

The interest for a comparison of $^{36}S+^{90,96}Zr$ fusion with the previous data for $^{40}Ca+^{90,96}Zr$ was stressed in the Introduction, and was actually one main motivation for the present measurements with the ^{36}S beam. A full intercomparison of the cross sections is shown by Fig. 5 which is the usual reduced plot of the excitation functions for all four systems. Barrier heights and radii are derived from the standard Akyüz-Winther potential; the data for $^{40}Ca+^{90,96}Zr$ have been slightly further renormalized to obtain a better overall agreement at the highest energies. This is anyway

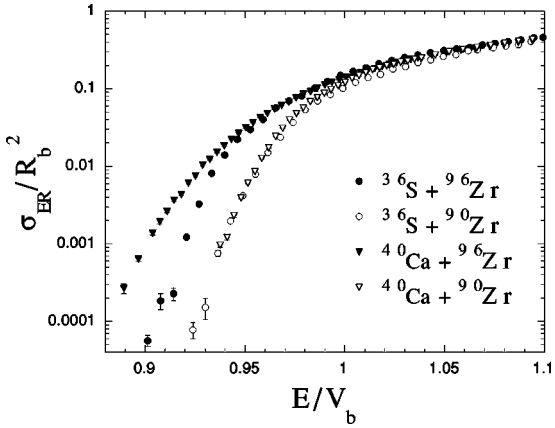

FIG. 5. Reduced plot of the excitation functions for the four systems $^{36}S+^{90,96}Zr$ (open and full circles) and $^{40}Ca+^{90,96}Zr$ [4] (open and full triangles).

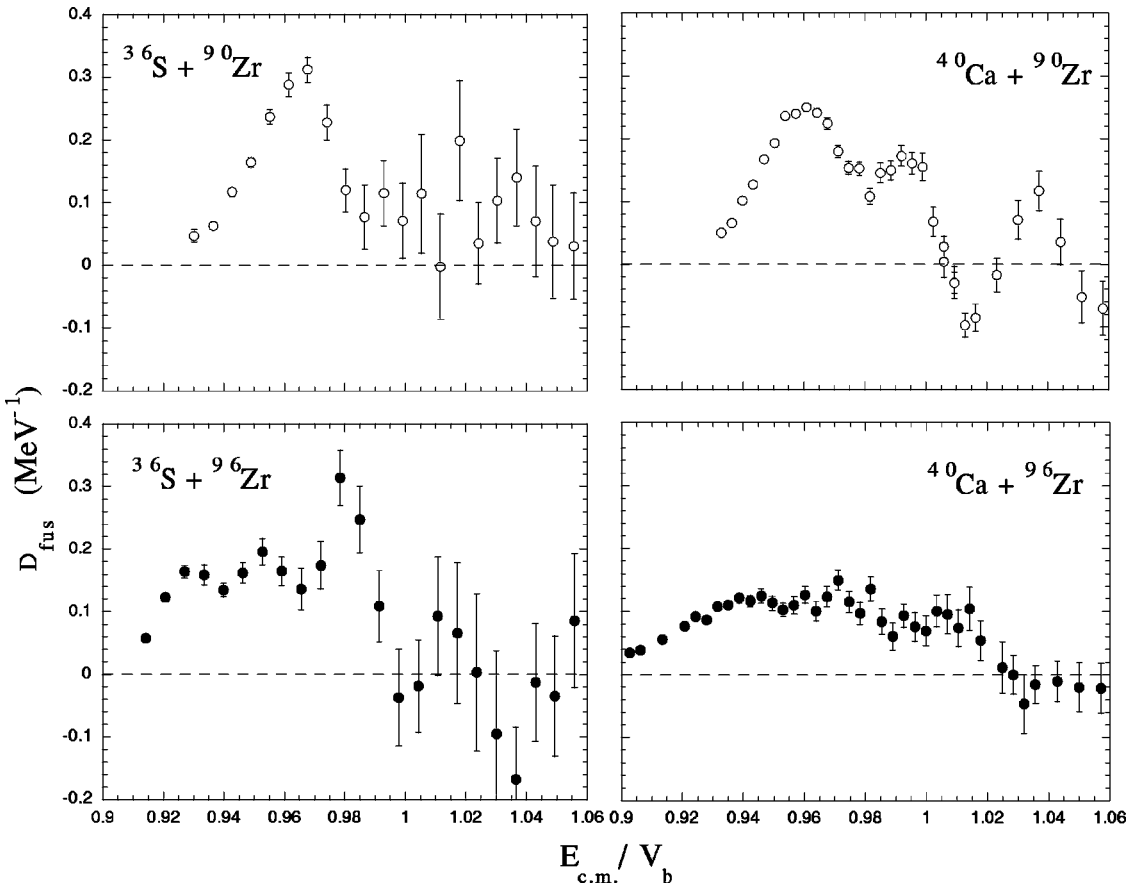

FIG. 6. Barrier distributions extracted for ^{40}Ca+^{90,96}Zr [4] and for ^{36}S+^{90,96}Zr, in an energy scale relative to the Coulomb barrier (see text).

within the uncertainty of the absolute cross section scale for our setup, and the observed systematics neither depends on this renormalization, nor does it change when using the potential parameters used for the CC calculations described in the text.

One notices that (1) the two cases with the ^{90}Zr target essentially fall on top of each other; (2) the sub-barrier cross sections of ^{36}S+^{96}Zr are larger by more than a factor of 10; (3) at low energies a further large enhancement is observed for ^{40}Ca+^{96}Zr whose sub-barrier excitation function, (4) is significantly less steep than the other three cases which are very similar to each other in this respect.

The four barrier distributions are reported in Fig. 6 in the energy scale relative to the Akyüz-Winther barriers V_b. The energy step used for extracting the Ca+Zr distributions is the same as in the original paper [4], i.e., $\Delta E = 1.75$ MeV ($\Delta E = 2.1$ MeV for $E \geqslant 1.02 V_b$). The error bars are smaller for the two Ca + Zr cases, especially at high energies, due (mainly) to the smaller statistical uncertainties of the cross section data, and to the slightly larger energy step compared to S+Zr ($\Delta E = 1.50$ MeV).

We notice that the two systems ^{36}S, ^{40}Ca+^{90}Zr (upper panels), which have almost coincident excitation functions, display similar barrier distributions as well, although the existence of a second peak at $E \simeq V_b$ for ^{36}S+^{90}Zr (predicted by the calculations, see Fig. 3) is not at all clear from the data having large error bars. Going to the ^{96}Zr targets (lower panels), both distributions get wider, as a consequence of the octupole strength in that nucleus. Furthermore, the distribution for ^{40}Ca+^{96}Zr is much flatter and extends to lower energies, compared to ^{36}S+^{96}Zr.

The calculations of Ref. [4] for ^{40}Ca+^{90,96}Zr have been repeated with CCFULL, in order to check the overall consistency of the analysis for all four systems. The results of CCFULL are essentially identical with the full CC calculations of Ref. [4], i.e., a very good (poor) fit of the excitation function and of the barrier distribution for ^{40}Ca+^{90}Zr (^{96}Zr).

We are led to the following considerations: the octupole vibration in ^{96}Zr has a strong effect on sub-barrier fusion, as predicted by the CC calculations described in Sec. III for the S+Zr systems. For ^{40}Ca+^{96}Zr the previous conclusion in Ref. [4] was that it is reasonable to suppose that the differences from ^{40}Ca+^{90}Zr come about from the large probabilities for few- and multinucleon transfer [20]. In view of the comparison with the new experimental findings for ^{36}S +^{90,96}Zr, we observe that the strong 3^- vibration of ^{96}Zr brings a strong contribution to the cross section enhancement and accounts for the excitation function of ^{36}S+^{96}Zr. Nevertheless, its effect is not strong enough to produce sub-barrier cross sections as large as measured for ^{40}Ca+^{96}Zr, nor does it produce a barrier distribution as wide as that

extracted for this system. Far below the barrier, couplings to neutron transfer channels may actually be the dominant factor in the fusion dynamics for $^{40}Ca+^{96}Zr$.

V. SUMMARY

We have presented here the results of the measurements of fusion-evaporation cross sections for $^{36}S+^{90,96}Zr$ at a number of energies near and below the Coulomb barrier. The relative accuracy of the experimental points has allowed us to extract the ''fusion barrier distributions'' as the second energy derivatives of the excitation functions. The data have been analyzed, within the coupled-channels model, by the code CCFULL which treats the excitation energies of the coupled modes correctly with full-order couplings. Good agreement is found, both for the cross sections and for the barrier distribution, for $^{36}S+^{90}Zr$, by considering the 2^+ excitation of the ^{36}S projectile and the lowest 2^+ and 3^- states of the target nucleus; going to two-phonon excitations does not improve the fit to the data. In the case of $^{36}S+^{96}Zr$ the two-phonon excitation of the strong octupole vibration in ^{96}Zr is found to be essential for reproducing the fusion excitation function; nevertheless, the barrier distribution, which is wider than for $^{36}S+^{90}Zr$, is only marginally fit by the calculations. Other important inelastic excitations do not exist and the possible effect of nucleon transfer channels is ruled out by *Q*-value considerations; changing the potential parameters destroys the good fit of the excitation function.

The comparison with the previous data on $^{40}Ca+^{90,96}Zr$ shows that the excitation functions of $^{36}S,^{40}Ca+^{90}Zr$ are very similar in the whole energy range and the two barrier distributions have similar overall shapes. The cross sections for $^{36}S+^{96}Zr$ are enhanced by a factor $\simeq 10$ below the barrier; a further large enhancement is found for $^{40}Ca+^{96}Zr$. These relative enhancements are mirrored in the fusion barrier distributions that become wider and flatter, surely as a consequence of the octupole vibration of ^{96}Zr. Its effect is clear and strong, but seems to be not sufficient to explain the very large cross sections found for $^{40}Ca+^{96}Zr$, where couplings to nucleon transfer channels may actually play a role at very low energies.

However, a full comprehension of the fusion dynamics near the barrier for medium-heavy systems it not yet at hand; this is shown, for the systems studied in the present work, by the inability of coupled-channels calculations to fit the shape of the barrier distribution of $^{36}S+^{96}Zr$ well. This situation seems to be analogous to the results of recent CC analyses of fusion data for $^{16}O+^{208}Pb$ [22].

ACKNOWLEDGMENTS

Grateful thanks are due to the XTU Tandem staff for careful and patient work during the experiments, and to G. Manente for professionally preparing targets of excellent quality. We are also grateful to G. Pollarolo for many discussions and for a critical reading of the manuscript.

[1] N. Rowley, G. R. Satchler, and P. H. Stelson, Phys. Lett. B **254**, 25 (1991).
[2] A. B. Balantekin and N. Takigawa, Rev. Mod. Phys. **70**, 77 (1998).
[3] M. Dasgupta, D. J. Hinde, N. Rowley, and A. M. Stefanini, Annu. Rev. Nucl. Part. Sci. **48**, 401 (1998).
[4] H. Timmers, D. Ackermann, S. Beghini, L. Corradi, J. H. He, G. Montagnoli, F. Scarlassara, A. M. Stefanini, and N. Rowley, Nucl. Phys. **A633**, 421 (1998).
[5] S. Beghini, C. Signorini, S. Lunardi, M. Morando, G. Fortuna, A. M. Stefanini, W. Meczynski, and R. Pengo, Nucl. Instrum. Methods Phys. Res. A **239**, 585 (1985).
[6] A. M. Stefanini, D. Ackermann, L. Corradi, J. H. He, G. Montagnoli, S. Beghini, F. Scarlassara, and G. F. Segato, Phys. Rev. C **52**, R1727 (1995).
[7] D. Ackermann *et al.*, Legnaro National Laboratory Annual Report 1993, Report LNL-INFN-081/94, p. 258.
[8] A. M. Stefanini, D. Ackermann, L. Corradi, D. R. Napoli, C. Petrache, P. Spolaore, P. Bednarczyk, H. Q. Zhang, S. Beghini, G. Montagnoli, L. Mueller, F. Scarlassara, G. F. Segato, F. Soramel, and N. Rowley, Phys. Rev. Lett. **74**, 864 (1995).
[9] Ö. Akyüz and A. Winther, in *Nuclear Structure and Heavy-Ion Physics, Proceedings of the International School of Physics ''Enrico Fermi,'' Course LXXVII, Varenna*, edited by R. A. Broglia and R. A. Ricci (North-Holland, Amsterdam, 1981).
[10] P. M. Endt, Nucl. Phys. **A521**, 1 (1990).
[11] L. P. Ekström and J. Lyttkens-Linden, Nucl. Data Sheets **67**, 579 (1992).
[12] S. Raman, C. H. Malarkey, W. T. Milner, C. W. Nestor, and P. H. Stelson, At. Data Nucl. Data Tables **36**, 1 (1987).
[13] R. H. Spear, At. Data Nucl. Data Tables **42**, 55 (1989).
[14] M. R. Bhat, Nucl. Data Sheets **82**, 547 (1997).
[15] K. Hagino, N. Rowley, and A. T. Kruppa, Comput. Phys. Commun. **123**, 143 (1999).
[16] H. Esbensen and S. Landowne, Phys. Rev. C **35**, 2090 (1987).
[17] H. Esbensen and B. B. Back, Phys. Rev. C **54**, 3109 (1996).
[18] K. Hagino, N. Takigawa, M. Dasgupta, D. J. Hinde, and J. R. Leigh, Phys. Rev. C **55**, 276 (1997).
[19] J. Leigh, M. Dasgupta, D. J. Hinde, J. C. Mein, C. R. Morton, R. C. Lemmon, J. P. Lestone, J. O. Newton, H. Timmers, J. X. Wei, and N. Rowley, Phys. Rev. C **52**, 3151 (1995).
[20] G. Montagnoli, S. Beghini, F. Scarlassara, G. F. Segato, L. Corradi, C. J. Lin, and A. M. Stefanini, J. Phys. G **23**, 1431 (1997).
[21] K. Hagino, S. Kuyucak, and N. Takigawa, Phys. Rev. C **57**, 1349 (1998).
[22] C. R. Morton, A. C. Berriman, M. Dasgupta, D. J. Hinde, J. O. Newton, K. Hagino, and I. J. Thompson, Phys. Rev. C **60**, 044608 (1999).